Dual Targeting of Apoptotic and Signaling Pathways in T-Lineage Acute Lymphoblastic Leukemia

Caner Saygin[1], Giorgia Giordano[1], Kathryn Shimamoto[1], Bart Eisfelder[1], Anika Thomas-Toth[2], Girish Venkataraman[3], Vijayalakshmi Ananthanarayanan[4], Tiffaney L. Vincent[5,6], Adam DuVall[1], Anand A. Patel[1], Yi Chen[7], Fenlai Tan[7], Stephen P. Anthony[7], Yu Chen[7], Yue Shen[7], Olatoyosi Odenike[1], David T. Teachey[5,6], Barbara L. Kee[3], James LaBelle[2], and Wendy Stock[1]

ABSTRACT

Purpose: Relapsed T-acute lymphoblastic leukemia (T-ALL) has limited treatment options. We investigated mechanisms of resistance to BH3 mimetics in T-ALL to develop rational combination strategies. We also looked at the preclinical efficacy of NWP-0476, a novel BCL-2/BCL-xL inhibitor, as single agent and combination therapy in T-ALL.

Experimental Design: We used BH3 profiling as a predictive tool for BH3 mimetic response in T-ALL. Using isogenic control, venetoclax-resistant (ven-R) and NWP-0476-resistant (NWP-R) cells, phosphokinase array was performed to identify differentially regulated signaling pathways.

Results: Typical T-ALL cells had increased dependence on BCL-xL, whereas early T-precursor (ETP)-ALL cells had higher BCL-2 dependence for survival. BCL-2/BCL-xL dual inhibitors were effective against both subtypes of T-lineage ALL. A 71-protein human phosphokinase array showed increased LCK activity in ven-R cells, and increased ACK1 activity in ven-R and NWP-R cells. We hypothesized that pre-TCR and ACK1 signaling pathways are drivers of resistance to BCL-2 and BCL-xL inhibition, respectively. First, we silenced LCK gene in T-ALL cell lines, which resulted in increased sensitivity to BCL-2 inhibition. Mechanistically, LCK activated NF-κB pathway and the expression of BCL-xL. Silencing ACK1 gene resulted in increased sensitivity to both BCL-2 and BCL-xL inhibitors. ACK1 signaling upregulated AKT pathway, which inhibited the pro-apoptotic function of BAD. In a T-ALL patient-derived xenograft model, combination of NWP-0476 and dasatinib demonstrated synergy without major organ toxicity.

Conclusions: LCK and ACK1 signaling pathways are critical regulators of BH3 mimetic resistance in T-ALL. Combination of BH3 mimetics with tyrosine kinase inhibitors might be effective against relapsed T-ALL.

Introduction

T-acute lymphoblastic leukemia (T-ALL) accounts for 15% of pediatric and 25% of adult ALL cases, and 90% of lymphoblastic lymphoma (LBL) cases (1). Nelarabine-containing pediatric-inspired multiagent chemotherapy can lead to 85% survival in children and young adults with T-ALL (2), but survival outcomes are inferior in older adults, and patients with relapsed or refractory (R/R) T-ALL/LBL have dismal outcomes (1). Treatment options are limited for patients with relapsed T-ALL/LBL, and a new class of drug has not been approved in over a decade. Only 20% to 30% of adults with relapsed T-ALL can achieve a second complete remission (CR) with current chemotherapy approaches, and even fewer can be subsequently rescued with potentially curative allogeneic hematopoietic cell transplantation (HCT), resulting in survival rates of only 10% to 20% (3). Therefore, alternative therapeutic approaches are urgently needed for patients with R/R T-ALL.

Resistance to cell death is a hallmark of blood cancers, which is regulated by the BCL-2 family of proteins (4). The prosurvival proteins BCL-2, BCL-xL, and MCL-1 act to sequester BAX and BAK, the two key cell death effector proteins, preventing their oligomerization and pore formation on the mitochondria. This balance is disrupted in cancer cells, which enables them to escape apoptosis even though they are primed to die from the cellular stresses that would kill their nonmalignant counterparts (5). BH3 mimetics can selectively bind to BCL-2 family of proteins and restore apoptosis in cancer cells (6). Venetoclax, a BCL-2-specific BH3 mimetic, has shown significant activity against acute myeloid leukemia (7), chronic lymphocytic leukemia (8), mantle cell lymphoma (9), and multiple myeloma (10). Since then, newer BH3 mimetics with dual BCL-2/BCL-xL activity have been developed. In hematologic malignancies, a switch in antiapoptotic protein dependence from BCL-2 to BCL-xL may lead to venetoclax resistance (11). Moreover, studies of T-ALL cell lines and patient samples showed antiapoptotic protein dependence on BCL-xL in typical precursor T-ALL, and BCL-2 dependence in early T precursor (ETP) ALL, highlighting the importance of dual BCL-2/BCL-xL targeting in this disease (12, 13). On the basis of these preliminary preclinical data in T-ALL and other leukemias, we conducted a multiinstitutional phase I dose-escalation study of venetoclax with navitoclax (the first BCL-2/BCL-xL dual inhibitor) and low-dose chemotherapy (vincristine, asparaginase, steroids) in patients with R/R B- and T-ALL (14). Although this study provided the proof-of-concept data for combination of BCL-2/BCL-xL inhibitor with chemotherapy in T-ALL, it is critical to understand the mechanisms of resistance to

[1]Section of Hematology/Oncology, Department of Medicine, University of Chicago, Chicago, Illinois. [2]Department of Pediatrics, University of Chicago, Chicago, Illinois. [3]Department of Pathology, University of Chicago, Chicago, Illinois. [4]Department of Pathology, Loyola University Medical Center, Chicago, Illinois. [5]The Children's Hospital of Philadelphia, Philadelphia, Pennsylvania. [6]University of Pennsylvania Perelman School of Medicine, Philadelphia, Pennsylvania. [7]Newave Pharmaceutical Inc., Pleasanton, California.

J. LaBelle and W. Stock contributed equally to this article.

Corresponding Author: Caner Saygin, Section of Hematology/Oncology, Department of Medicine, University of Chicago, Chicago, IL 60637. Email: caner.saygin@uchicagomedicine.org

Clin Cancer Res 2023;29:3151–61

doi: 10.1158/1078-0432.CCR-23-0415

Translational Relevance

Relapsed T-lineage acute lymphoblastic leukemia (T-ALL) has dismal prognosis, for which a new class of drug has not been approved in over a decade. In this preclinical study, we demonstrated that typical precursor T-ALL cells depend on BCL-xL for survival, whereas early T-precursor ALL cells depend on BCL-2. The novel BCL-2/BCL-xL dual inhibitor NWP-0476 was effective against both subtypes of T-ALL. We identified LCK and ACK1 signaling pathways as drivers of resistance to BH3 mimetics, which can be effectively targeted with tyrosine kinase inhibitors (TKI), dasatinib or ponatinib. Mechanistically, LCK-mediated resistance to venetoclax was driven by NF-κB pathway and upregulation of BCL-xL expression. ACK1 signaling upregulated AKT pathway, which inhibited BAD. In T-ALL xenograft models, combination of NWP-0476 and dasatinib demonstrated synergy without major organ toxicity. Our results have immediate clinical applications and clinical trials investigating the combination of BH3 mimetics with TKIs are at different stages of development.

BH3 mimetics in this disease. Targeting the drivers of BH3 mimetic resistance may offer new synergistic combinations and improve outcomes for R/R T-ALL.

Given the importance of BCL-2 and BCL-xL pathways for survival of T-lymphoblasts, we set out to investigate the patterns of response and mechanisms of resistance to BH3 mimetics in T-ALL. Using cell lines, primary patient cells and patient-derived xenograft (PDX) models, we demonstrated that BH3 profiling can predict response to BH3 mimetics in T-lineage ALL, and dual BCL-2/BCL-xL inhibition can target both T- and ETP-ALL. We also used a next-generation potent BCL-2/BCL-xL inhibitor, NWP-0476, which has a modified structure with fine-tuned BCL-xL activity to minimize the platelet toxicity observed with navitoclax (15). Our phospho-kinase profiling revealed that pre-T-cell receptor (pre-TCR) and ACK1 signaling pathways were upregulated with acquired resistance to BCL-2 and BCL-xL inhibitors, respectively. Therefore, we hypothesized that LCK and ACK1 signaling pathways are drivers of BH3 mimetic resistance in T-ALL, and dual inhibition of signaling and antiapoptotic pathways synergistically suppresses the growth of T lymphoblasts. We tested this hypothesis by inhibiting LCK and ACK1 with shRNA and pharmacologic approaches, which sensitized cells to BH3 mimetics. Using both *in vitro* and *in vivo* models of T-ALL, we demonstrated the efficacy of combining NWP-0476 with tyrosine kinase inhibitors (TKI; dasatinib and ponatinib) in T-ALL. These data provide new approaches to overcome BH3 mimetic resistance in T-ALL, and pave the way for future studies looking at TKI plus BH3 mimetic combinations.

Materials and Methods

Human T-ALL cell lines, primary cells, and PDX lines

Human T-ALL cell lines ALL-SIL (RID:CVCL_1805), MOLT4 (RRID:CVCL_0013), and MOLT16 (RRID:CVCL_1424) were purchased from ATCC, and cultured in RPMI supplemented with 10% heat-inactivated FBS and 2 mmol/L L-glutamine. All cell lines were authenticated with STR assay and mycoplasma-tested on an annual basis. The primary T-ALL cells were obtained from 20 patients with typical precursor T-ALL and 6 patients with ETP-ALL who were treated at the University of Chicago and written informed consent has been obtained from each patient according to our Institutional Review Board–approved research protocols in accordance with the Declaration of Helsinki (Supplementary Table S1). Blood or bone marrow samples containing high percentages of leukemic blasts were subjected to Ficoll gradient centrifugation and the mononuclear cell layer was collected. Primary patient cells were cultured in RPMI1640 supplemented with 2 mmol/L L-glutamine, 10% FBS, and insulin–transferrin–selenium. T-ALL PDX model was developed by engraftment of primary cells into NOD-SCID IL2Rg^{null} (NSG) mice as described previously (16).

Cell viability assays

Cells were incubated for 48 hours in the presence of increasing concentrations of single or combination drug treatments. Cell viability was assayed by adding Cell Counting Kit-8 (CCK-8; Dojindo Molecular Technologies, Inc.) to the cell culture for the last 4 hours, and quantitated using Bio Tek Synergy H4 plate reader and Gen5 software as described previously (17). IC_{50} dose was defined as the IC_{50}, calculated using nonlinear fitted dose–response curves in GraphPad Prism v.9.0 (RRID:SCR_002798). Experiments were done in triplicate. For *in vitro* experiments looking at the synergy between BH3 mimetics and TKIs, zero interaction potency (ZIP) synergy scores were calculated using SynergyFinder v.3.0 (https://doi.org/10.1093/nar/gkac382; RRID:SCR_019318). Venetoclax, navitoclax, A-1155463, dasatinib, ponatinib, BMS 345541, and capivasertib were obtained from Selleck Chemicals. NWP-0476 was provided by Newave Pharmaceutical, lnc.

BH3 profiling

BH3 profiling is a functional assay that can identify selective antiapoptotic protein dependencies (BCL-2, BCL-xL, or MCL1) in different T-ALL cell lines or primary cells. In this assay, mitochondrial outer membrane permeabilization (MOMP) is a readout for apoptotic activation, which we assessed as described previously (18). In plate-based fluorimetry method, BH3 peptides were plated in triplicate on a black 384-well plate at following concentrations: BAD, HRK, and MS1 were used at 1 μmol/L concentration, whereas BIM and BID were also plated at different concentrations for titration assays (0–100 μmol/L). Cells were gently permeabilized with 0.005% digitonin and incubated with the JC1, a fluorescent mitochondrial dye. The cells were added on top of the peptides at 2×10^4 cells per well. An intact mitochondrial membrane resulted in dye accumulation with positive fluorescent signal, whereas membrane depolarization resulted in a decrease in fluorescent intensity. The fluorescent intensities of the wells were measured on the Bio Tek Synergy H4 plate reader at an excitation of 545 nmol/L and an emission of 590 nmol/L over 3 hours. By using peptides that specifically engage with anti-apoptotic proteins, the degree of apoptotic priming (i.e., BIM dose-titration assay) and sensitivity to individual BCL-2 family of proteins were quantified. Percent mitochondrial depolarization was calculated by normalization to the solvent only control DMSO and the positive control alamethicin. In flow cytometry–based BH3 profiling by intracellular staining (iBH3), MOMP was assessed with cytochrome *c* loss from the mitochondria of digitonin-permeabilized blasts.

Receptor tyrosine kinase (RTK) array

For the phospho-RTK activation study, a RayBio antibody array against 71 unique tyrosine kinases was used according to the manufacturer's protocol (Raybio AAH-PRTK-1–4). Cell lysates (1 mg) from isogenic ALL-SIL control, and venetoclax-resistant and NWP-resistant cells were added to each membrane. Spot quantitation was done using ImageJ/Fiji (RRID:SCR_003070), and mean densities were calculated for each spot in a duplicate and normalized to the densities

of background and positive control dots. Relative expression levels of different phospho-kinases were calculated and plotted as a heatmap.

Immunoblotting

Whole-cell protein extracts were obtained by lysis of cells in RIPA buffer mixed with 1 mmol/L sodium orthovanadate, protease, and phosphatase inhibitor cocktails. Proteins in lysates (20–50 μg total protein) were resolved by 10% SDS-PAGE and transferred to nitrocellulose membrane. Membranes were incubated overnight at 4°C with primary antibodies against pACK1 (Y284; 1:500; Abcam, ab74091), ACK1 (1:500; Abcam, ab185726), pZAP70 (Y319; 1:500; Cell Signaling Technology, #2701), ZAP70 (1:500; Cell Signaling Technology, #3165), pLCK (Y505; 1:500; Cell Signaling Technology, #2751), pLCK (Y394; 1:500; R&D Systems, MAB7500), LCK (1:1,000; Santa Cruz Biotechnology, sc-433), pLYN (Y396; 1:500; Thermo Fisher Technology, MA5–35882), LYN (1:1,000; Cell Signaling Technology, #2796), pFYN (Y420; 1:500; Cell Signaling Technology), FYN (1:1,000; Cell Signaling Technology, #4023), tubulin (1:2,000; Cell Signaling Technology), histone H3 (1:2,000; Cell Signaling Technology, #4499), BCL-2 (1:1,000; Cell Signaling Technology, #4223), BCL-xL (1:1,000; Cell Signaling Technology, #2764), p-NF-κB p65 (1:500; Cell Signaling Technology, #3033), NF-κB p65 (1:500; Cell Signaling Technology, #8242), p-IκBα (1:500; Cell Signaling Technology, #2859), IκBα (1:500; Cell Signaling Technology, #4814), p-AKT (S473; 1:500; Cell Signaling Technology, #4060), AKT (1:1,000; Cell Signaling Technology, #9272), p-BAD (S136; 1:500; Cell Signaling Technology, clone D25H8), and BAD (1:1,000; Cell Signaling Technology, #9292). Secondary anti-mouse or anti-rabbit IgG antibodies conjugated to HRP (1:2,000; Thermo Fisher Scientific) were used, and immunoreactive bands were visualized using the ECL Plus from Pierce.

Lentivirus production and infection

Lentiviral shRNAs for LCK and ACK1 transductions were prepared as we reported previously (19). HEK 293T/17 cells (RRID: CVCL_1926) were cotransfected with the packaging vectors from Dharmacon Trans-Lentiviral shRNA Packaging System (Horizon, lnc.), and lentiviral vectors directing expression of shRNA specific to LCK (TRCN0000001598, TRCN0000001600, TRCN0000055434), ACK1/TNK2 (TRCN0000002038, TRCN0000002040), a nontargeting (NT) control shRNA (SHC002), and overexpression vector for LCK and ACK1 (Precision LentiORF collection from Horizon, lnc.). Media of the HEK 293T/17 cells were changed 24 hours after transfection, and viral particles were harvested at 48 hours via concentration with polyethylene glycol precipitation. Viral infections were performed in ALL-SIL, MOLT4, and MOLT16 cell lines, and after transduction, cells were selected using 2 to 5 μg/mL puromycin for shRNA constructs and blasticidin for overexpression constructs.

RNA sequencing

Total RNA was purified from MOLT4 NT control, LCK knockdown, and ACK knockdown cell lines by using QIAGEN RNeasy Mini Kit (Qiagen, 74104). Total RNA library was constructed with an Illumina TrueSeq Stranded mRNA Library Prep Kit and sequenced using the NovaSeq 6000 platform (2 × 100-bp paired-end reads). Transcriptomic reads were aligned to the reference human genome (GRCh38) using HISAT2, provided by Galaxy software (RRID: SCR_006281; ref. 20). Differential gene expression analysis was performed with the Limma package. Ingenuity pathway analysis (Qiagen, Inc.) was used to analyze gene networks for differentially expressed genes with a log2 fold change >1 or <1, and an adjusted *P*-value <0.1.

Immunocytochemistry

To visualize the nuclear translocation of NF-κB in ALL-SIL cells, isogenic control and venetoclax-resistant cells were plated on poly-L-lysine coated coverslips placed in a 6-well plate. After 12 to 16 hours, the cells were fixed for 15 minutes with 4% paraformaldehyde at room temperature and washed three times with PBS. Then they were blocked in 5% goat serum with 1 mg/mL BSA and 0.3% TritonX-100 for 2 hours. Rabbit anti-human NF-κB p65 antibody (D14E12, Cell Signaling Technology) was used to stain cells overnight at 4°C. The following day, cells were washed three times with PBS for 5 minutes, and A488-conjugated goat anti–rabbit secondary antibody (Invitrogen) was applied for 1 hour at room temperature. After secondary antibody incubation, cells were washed three times with PBS for 5 minutes each and counterstained with DAPI for 5 minutes. Afterward, cells were washed three times with PBS for 5 minutes each. The coverslips were mounted using anti-fade fluorescence mounting medium (Abcam, ab104135), and cells were imaged using a Leica TCS SP8 Confocal/Multi-Photon high-speed upright microscope. Nuclear to cytoplasmic NF-κB p65 ratio was calculated using ImageJ.

Chromatin immunoprecipitation (ChIP)

ChIP assay was performed using the SimpleChIP Enzymatic Chromatin IP Kit (Cell Signaling Technology, #9003) according to the manufacturer's instructions. Briefly, venetoclax-resistant ALL-SIL cells (0.5×10^6 cells/mL) were treated with 1% formaldehyde to cross-link DNA binding proteins to genome DNA and cross-linking was stopped by the addition of glycine. After washing with ice-cold PBS several times, the cells were resuspended and 0.5 μL of micrococcal nuclease was added to digest DNA to length of 150 to 900 bp. Next, 0.5M EDTA was added to stop digestion and cells were sonicated to break nuclear membrane by Sonifier 250A. Each 10 μg of chromatin DNA was immunoprecipitated with rabbit IgG or rabbit anti-human NF-κB p65 antibody (D14E12, Cell Signaling Technology) at 4°C overnight. After incubation, 30 μL of protein G magnetic beads were added to immunoprecipitating complexes and incubated for 2 hours at 4°C. The immunoprecipitating complex was eluted with 150 μL of ChIP elution buffer and formaldehyde cross-linking was reversed by adding NaCl and Proteinase K and by heating at 65°C for 2 hours. Genomic DNA was purified and analyzed by PCR, using BCL-xL specific primers (5′-GATCCCCATGGCAGCAGTAAAGCAAG-3′ and 5′-CCCCATCCCGGAAGAGTTCATTCACT-3′).

Protein immunoprecipitation

For protein immunoprecipitation, cells were lysed in cell lysis buffer (Cell Signaling Technology, #9803). The lysates were spun at 14,000 × *g* for 10 minutes at 4°C. Supernatants were incubated with rabbit anti-human BAD antibody (Cell Signaling Technology, #9292) and incubated with rotation for 2 hours at 4°C. Protein A agarose beads (Cell Signaling Technology, #9863) were added to lysates (10–30 μL of 50% bead slurry), which were subsequently incubated with rotation for 2 hours at 4°C. The beads were then washed three to four times at 4°C, and the pellets were resuspended with 20 μL 3× SDS sample buffer. Samples were heated to 95 to 100°C for 5 minutes and centrifuged for 1 minute at 14,000 × *g*. Immunoblotting was performed using the indicated primary antibodies described above.

Xenograft studies

All mouse procedures were approved by the University of Chicago Institutional Animal Care and Use Committee and carried out with adherence to all appropriate guidelines and using a complication scoring system to minimize animal suffering. NSG mice were engrafted

via tail vein injection with 500,000 luciferase-transduced T-ALL PDX cells, and randomized to four treatment arms the following day: vehicle control, NWP-0476 daily via oral gavage, dasatinib daily via oral gavage, and NWP-0476 plus dasatinib daily via oral gavage (5 mice in each group). After 3 weeks of treatment, mice were monitored weekly by intraperitoneal luciferin injection and bioluminescence imaging. Overall survival (OS) of four groups was compared with Kaplan–Meier analysis and log-rank test. Deceased mice underwent necropsy, and their organs (liver, kidney, heart, gut) were resected for histopathologic analysis of drug toxicity.

Statistical analysis

Statistical analysis was conducted using GraphPad Prism, v9.0 (RRID: SCR_002798). Grouped data are presented as mean ± SD. Differences between groups were assessed using Kruskal–Wallis test, and *P*-values are detailed in the text and figure legends.

Data availability

Relevant details of experimental data are provided in Supplementary Materials and Methods. Any additional data can be provided upon reasonable request from the Corresponding Author.

Results

Dynamic BH3 profiling identifies apoptotic dependencies and predicts response to BH3 mimetics in T-lineage ALL

To identify the most effective strategy to target different types of T-lineage ALL, we tested four BH3 mimetic compounds that differed from each other in their antiapoptotic protein specificity: venetoclax (BCL-2 inhibitor), NWP-0476 (a novel BCL-2/BCL-xL inhibitor), navitoclax (BCL-2/BCL-xL inhibitor), and A-1155463 (BCL-xL inhibitor; **Fig. 1A**). Next, we studied the sensitivity of 20 different T-ALL and 6 different ETP-ALL primary patient cells to treatment with these BH3 mimetics (**Fig. 1B**; Supplementary Fig. S1A; Supplementary Table S1). Typical T-ALL samples showed higher sensitivity to BCL-xL targeting agents, whereas ETP-ALL samples were more sensitive to BCL-2 inhibition (**Fig. 1B** and **C**). Dual BCL-2/BCL-xL inhibitors, NWP-0476 and navitoclax, were effective against both subtypes of T-lineage ALL. Next, we performed BH3 profiling to identify selective antiapoptotic protein dependencies in these samples. In this functional assay, cells are treated with BH3 peptides targeting specific members of the BCL-2 family of proteins, and the degree of mitochondrial depolarization is measured by the release of JC1 dye (**Fig. 1D**). In all patient samples, BH3 profiles correlated with the differential sensitivity to BCL-2 versus BCL-2/BCL-xL inhibition as evidenced by increased response to HRK stimulation (BCL-xL targeting) in typical T-ALL and higher BAD (BCL-2 and BCL-xL targeting) minus HRK values ("BAD-HRK" indicating BCL-2 dependence) in ETP-ALL samples (**Fig. 1E**; Supplementary Fig. S1B). Collectively, these results indicate that BCL-2/BCL-xL dual inhibitors have a broad spectrum of activity against both T- and ETP-ALL, and BH3 profiling can be a valuable predictive tool for BH3 mimetic treatment response.

Pre-TCR and ACK1 signaling pathways are involved in acquired resistance to BH3 mimetics in T-ALL

To gain insights into the mechanisms by which resistance to BH3 mimetics emerges in T-ALL, we generated isogenic control, venetoclax-resistant (ven-R), and NWP-0476-resistant (NWP-R) ALL-SIL cell lines by passaging these cells with respective drugs *in vitro*. ALL-SIL ven-R cells exhibit 16-times higher IC_{50} for venetoclax [23.7 µmol/L

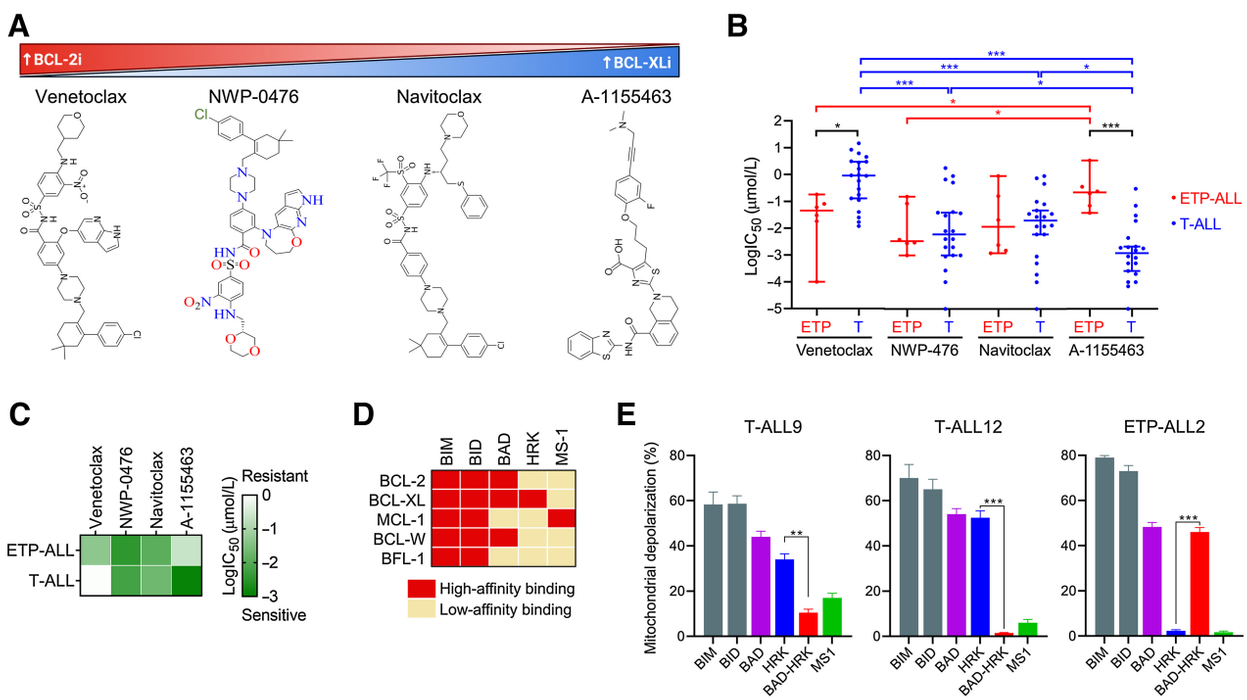

Figure 1.

BH3 profiling predicts response to BH3 mimetics in T-lineage ALL. **A,** Chemical structures for BH3 mimetics with differential binding to BCL-2 and BCL-xL antiapoptotic proteins. **B,** Whisker plots showing log(IC_{50}) values for ETP and typical T-ALL primary patient cells treated with BH3 mimetics. **C,** Heatmap depicting sensitivities of ETP- and T-ALL patient samples to different BH3 mimetics. **D,** Heatmap showing the specificities of BH3 peptides for different BCL-2 family of proteins. **E,** BH3 profiling of primary cells from ETP- and T-ALL patients (*, $P < 0.05$; **, $P < 0.01$; ***, $P < 0.001$).

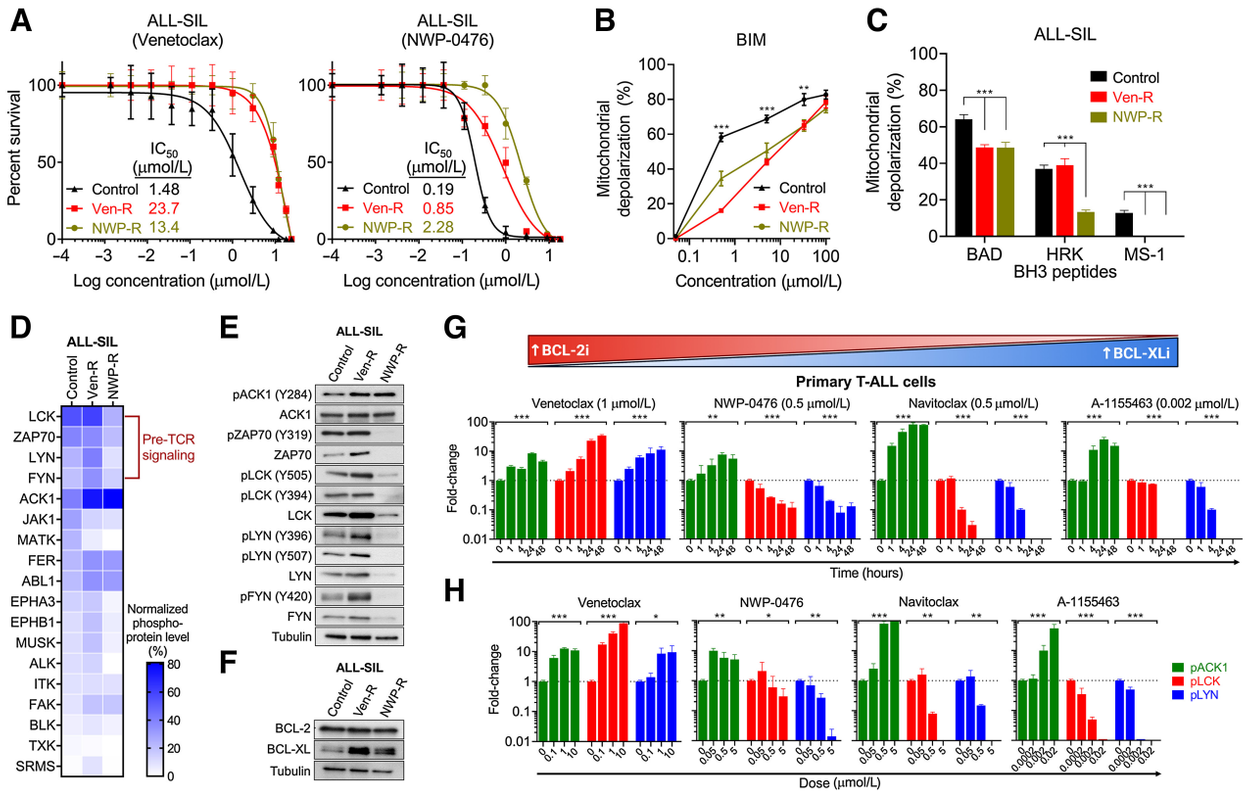

Figure 2.

LCK and ACK1 signaling pathways are associated with resistance to BH3 mimetics in T-ALL. **A,** Generation of isogenic control, ven-r, and NWP-R ALL-SIL T-ALL cell lines. **B,** BIM titrating assay showing apoptotic priming for ALL-SIL control, ven-R, and NWP-R cells. **C,** BH3 profiling of isogenic control and BH3 mimetic-resistant cell lines. **D,** Heatmap depicting the most differentially expressed phospho-kinases between ALL-SIL control, ven-R, and NWP-R cells. **E,** Immunoblots validate the phospho-kinase array results. **F,** Immunoblots showing the expression of BCL-2 and BCL-xL levels in ALL-SIL ven-R and NWP-R cells as compared with parental controls. **G,** Bar graphs showing changes in phospho-kinase levels over 48 hours after BH3 mimetic treatment of primary T-ALL cells. Changes were normalized to the levels of proteins on day 0. **H,** Bar graphs showing changes in phospho-kinase levels after 24 hours of treatment with increasing doses of BH3 mimetics in primary T-ALL cells. Changes were normalized to untreated cells (*, $P < 0.05$; **, $P < 0.01$; ***, $P < 0.001$).

(95% CI, 20.6–25.4 μmol/L) vs. 1.48 μmol/L (95% CI, 1.2–0.7 μmol/L)], and NWP-R cells exhibit 12-times higher IC_{50} for NWP-0476 [2.28 μmol/L (95% CI, 2–2.5 μmol/L) vs. 0.19 μmol/L (95% CI, 0.1–0.3 μmol/L)] compared with their parental controls (**Fig. 2A**). Ven-R and NWP-R cells demonstrated decreased mitochondrial depolarization in a BIM titration assay, a readout for decreased apoptotic priming (**Fig. 2B**). Ven-R cells had decreased response to BCL-2 targeting peptide BAD, and NWP-R cells had decreased response to both BCL-2 and BCL-xL targeting peptides, indicating the correlation between BH3 profiling and BH3 mimetic response (**Fig. 2C**; Supplementary Fig. S2A–S2D). Next, we analyzed the differentially regulated signaling pathways between the control versus resistant cells by using a 71-protein human phosphokinase array (**Fig. 2D**). Pre-TCR signaling pathway was upregulated in ven-R cells, including LCK, ZAP70, LYN, and FYN kinases (**Fig. 2D** and **E**). These kinases were downregulated in NWP-R cells compared with the parental control cells. In addition, increased ACK1 (TNK2) signaling was observed in both ven-R and NWP-R cells compared with the parental control cells. We also looked at the expression levels of antiapoptotic proteins in these isogenic cell lines, and showed upregulation of BCL-xL in ven-R cells (**Fig. 2F**). To validate these results in patient samples, we treated primary cells from 3 different patients (T-ALL3, T-ALL9, T-ALL12) with the predetermined IC_{50} doses of BH3 mimetics over 48 hours (**Fig. 2G**), and with escalating doses of drugs for 24 hours (**Fig. 2H**). Of note, cells treated with the four BH3 mimetics were 50% viable at 4-hour time point, confirming the quick onset of action for these compounds (Supplementary Fig. S3A). Viable cells were selected with the Dead Cell Removal Kit prior to lysis and subsequent Western blot experiments (Miltenyi Biotech, 130–090–101). BCL-2 inhibition enriched for cells that have upregulated pre-TCR signaling (pLCK and pLYN), whereas BCL-xL inhibition led to the persistence of cells with very low pre-TCR signaling activity (**Fig. 2G** and **H**; Supplementary Fig. S3B–S3D). Similar to the cell line data, increased ACK1 signaling was observed with all treatments, and was more pronounced in cells treated with BCL-xL inhibitors. These data suggest that in T-ALL, LCK and ACK1 signaling are associated with resistance to BCL-2 and BCL-xL inhibitors, respectively.

LCK drives venetoclax resistance in T-ALL by upregulating NF-κB signaling and BCL-xL expression

Given the increased activity of pre-TCR signaling in venetoclax-resistant cell lines and primary patient cells, we sought to investigate whether inhibition of LCK is sufficient to sensitize cells to BCL-2 inhibition. ALL-SIL cell line did not tolerate LCK silencing as the cells could not recover from lentiviral transduction. Therefore, we used MOLT4 and MOLT16 cell lines, which had high baseline LCK activity

and venetoclax resistance, for LCK knockdown (KD) studies. First, we silenced LCK in MOLT4 and MOLT16 T-ALL cell lines by using three nonoverlapping shRNA constructs (**Fig. 3A**; Supplementary Fig. S4A). MOLT4 and MOLT16 cells with LCK KD had increased sensitivity to BCL-2 inhibition (with venetoclax, NWP-0476, or navitoclax) when compared with their respective control cells transduced with NT shRNA control (**Fig. 3B**; Supplementary Fig. S4B–S4D). However, LCK KD cells were less sensitive to BCL-xL–specific inhibitor A-1155463. BH3 profiling revealed increased mitochondrial depolarization after BIM treatment in LCK-silenced MOLT4 cells when compared with NT control, indicating decreased apoptotic threshold in LCK KD cells (**Fig. 3C**). Concomitantly, mitochondria of LCK KD cells had increased sensitivity to stimulation with BAD peptide, but decreased sensitivity to HRK peptide, suggesting increased apoptotic vulnerability for BCL-2 targeting but decreased sensitivity to BCL-xL targeting (**Fig. 3D**).

To understand the mechanisms by which LCK signaling regulates resistance to BCL-2 inhibition, we performed RNA sequencing (RNA-seq) to compare the transcriptomic profiles of NT control versus LCK KD and control versus ven-R cells. Genes that had more than 2-fold change with an adjusted-*P*-value corrected for FDR <0.1 were further studied with ingenuity pathway analysis (RRID:SCR_008653). Upon LCK KD, genes regulating cell survival and tumor cell invasion were significantly downregulated, whereas genes implicated in lymphoid cell apoptosis were upregulated (**Fig. 3E**; Supplementary Fig. S5A). Next, we investigated genes that were upregulated in ven-R cells and downregulated in LCK KD cells to identify the shared genes that may have a role in LCK-driven ven-R phenotype (**Fig. 3F** and **G**). Among the 14 genes in common, *NFKB1* and genes that are transcribed under the control of transcription factor NF-κB (e.g., *IL32*, *BHLHE40*, *PECAM1*) were identified. We further validated RNA-seq data at the protein level by showing increased NF-κB pathway activity in ALL-SIL ven-R cells compared with isogenic control cells, and downregulated NF-κB signaling in MOLT4 LCK KD cells compared with NT control (**Fig. 3H**). Increased NF-κB signaling was associated with increased BCL-xL expression, which correlates with increased BCL-xL dependence in ven-R or LCK-high T-ALL cells. Next, we successfully transduced LCK into ALL-SIL cells (**Fig. 3I**). Upon LCK overexpression (OE), NF-κB signaling and BCL-XL expression were upregulated. LCK-overexpressing ALL-SIL cells became more resistant to venetoclax when compared with control cells transduced with empty vector (**Fig. 3J**). To interrogate NF-κB pathway activity in the context of venetoclax resistance, we stained ALL-SIL control and ven-R cells by immunocytochemistry (**Fig. 3K**). Nuclear:cytoplasmic ratio of NF-κB staining was significantly higher in ven-R cells, suggesting increased NF-κB activity (**Fig. 3L**). Beause LCK KD or OE altered NF-κB activity with changes in BCL-xL expression, we examined whether NF-κB was bound to the BCL-xL promoter to drive its expression. To this end, we performed ChIP assay and showed that NF-κB p65 was bound to the BCL-xL promoter in ALL-SIL ven-R cells (**Fig. 3M**). Finally, we tested the efficacy of NF-κB pathway inhibition by using the selective IκB kinase (IKK) inhibitor, BMS 345541. ALL-SIL ven-R cells, and MOLT4 control cells were more susceptible to IKK inhibition compared with control and LCK KD cells, respectively (Supplementary Fig. S5B). This differential response to BMS 345541 correlates with the NF-κB pathway dependence of respective cells. We also observed synergy between venetoclax and BMS 345541 in MOLT4 cells and primary human T-ALL cells, assessed with the ZIP method (Supplementary Fig. S5C). Upon IKK inhibition, BCL-xL expression was downregulated in ALL-SIL ven-R cells (Supplementary Fig. S5D). Altogether, these data indicate that venetoclax resistance in T-ALL is driven by LCK pathway, which signals through NF-κB to upregulate BCL-xL expression.

ACK1 regulates BH3 mimetic sensitivity in T-ALL via AKT-mediated phosphorylation of BAD

On the basis of the preliminary data showing increased ACK1 (TNK2) activity in ven-R and NWP-R cells, we investigated whether ACK1 inhibition can sensitize T-ALL cells to BH3 mimetics. We silenced ACK1 in MOLT4 and MOLT16 T-ALL cell lines by using two nonoverlapping shRNA constructs (**Fig. 4A**; Supplementary Fig. S6A). MOLT4 and MOLT16 cells with ACK1 KD had increased sensitivity to both BCL-2 and BCL-xL inhibition when compared with their respective control cells transduced with NT shRNA control (**Fig. 4B**; Supplementary Fig. S6B–S6D). BH3 profiling revealed increased apoptotic sensitivity of the mitochondria from ACK1 KD cells in BIM titration assay (**Fig. 4C**). In addition, ACK1 KD cells had increased sensitivity to stimulation with BAD and HRK peptides, suggesting increased apoptotic vulnerability for both BCL-2 and BCL-xL targeting (**Fig. 4D**).

Previous reports showed that ACK1 exerts its growth-promoting effects by direct phosphorylation of AKT (21, 22). AKT phosphorylates BAD at S136 locus, which blocks the interaction of BAD with anti-apoptotic BCL-2 and BCL-xL proteins (23). To gain insights into the ACK1-mediated resistance to BCL-2 and BCL-xL inhibition in T-ALL, we interrogated these pathways in our cell lines. By Western blot analysis, we found increased p-AKT activity in NWP-R cells, and these cells had higher levels of p-BAD (S136), which is known to be a downstream target of AKT signaling (**Fig. 4E**). Upon ACK1 KD, p-AKT and p-BAD (S136) levels were reduced and these cells were less sensitive to AKT inhibition by capivasertib (**Fig. 4E**; Supplementary Fig. S6E). We also observed synergy between NWP-0476 and capivasertib in MOLT4 cells and primary human T-ALL cells, assessed with the ZIP method (Supplementary Fig. S6F). To demonstrate that ACK1 is the driver of BCL-2/BCL-xL inhibitor resistance through AKT-BAD signaling pathway, we transduced ACK1 into ALL-SIL cells (**Fig. 4F**). ACK1 OE led to increased p-AKT and p-BAD levels, as well as increased resistance to treatment with venetoclax and NWP-0476 (**Fig. 4F** and **G**). On the contrary, treatment with AKT inhibitor capivasertib led to decreased phosphorylation of BAD at S136 (**Fig. 4H**). To confirm the interaction between BAD and BCL-2/BCL-xL in the context of BH3 mimetic resistance, we pulled down BAD protein in isogenic ALL-SIL control and NWP-0476-resistant cell lines (**Fig. 4I**). In control cells that are sensitive to NWP-0476, BAD protein immunoprecipitation showed interaction with BCL-2 and BCL-xL as expected. However, NWP-R cells had higher levels of p-BAD, which did not interact with BCL-2 and BCL-xL. Collectively, these data demonstrate that ACK1 upregulates the activity of AKT pathway in T-ALL, which phosphorylates BAD to prevent its interaction with BCL-2 and BCL-xL antiapoptotic proteins.

Combination of BH3 mimetics and TKIs offers synergistic antileukemic activity in T-ALL

On the basis of our mechanistic data showing the role of LCK and ACK1 signaling in BH3 mimetic resistance in T-ALL, we sought to investigate the preclinical activity of combined BH3 mimetic plus TKI therapy in T-ALL. Dasatinib is a broad-spectrum kinase inhibitor, targeting both LCK (KD_{50} = 20 nmol/L) and ACK1 (KD_{50} = 5.60 nmol/L). Ponatinib is a newer TKI that also targets both of these kinases effectively (Supplementary Fig. S7A). In T-ALL primary cells, the combination of venetoclax or NWP-0476 with dasatinib demonstrated synergy in both treatment-naïve (T-ALL9, T-ALL12) and chemotherapy-refractory (T-ALL7, T-ALL20) patient samples when assessed with ZIP method (**Fig. 5A** and **B**; Supplementary Fig. S7B–

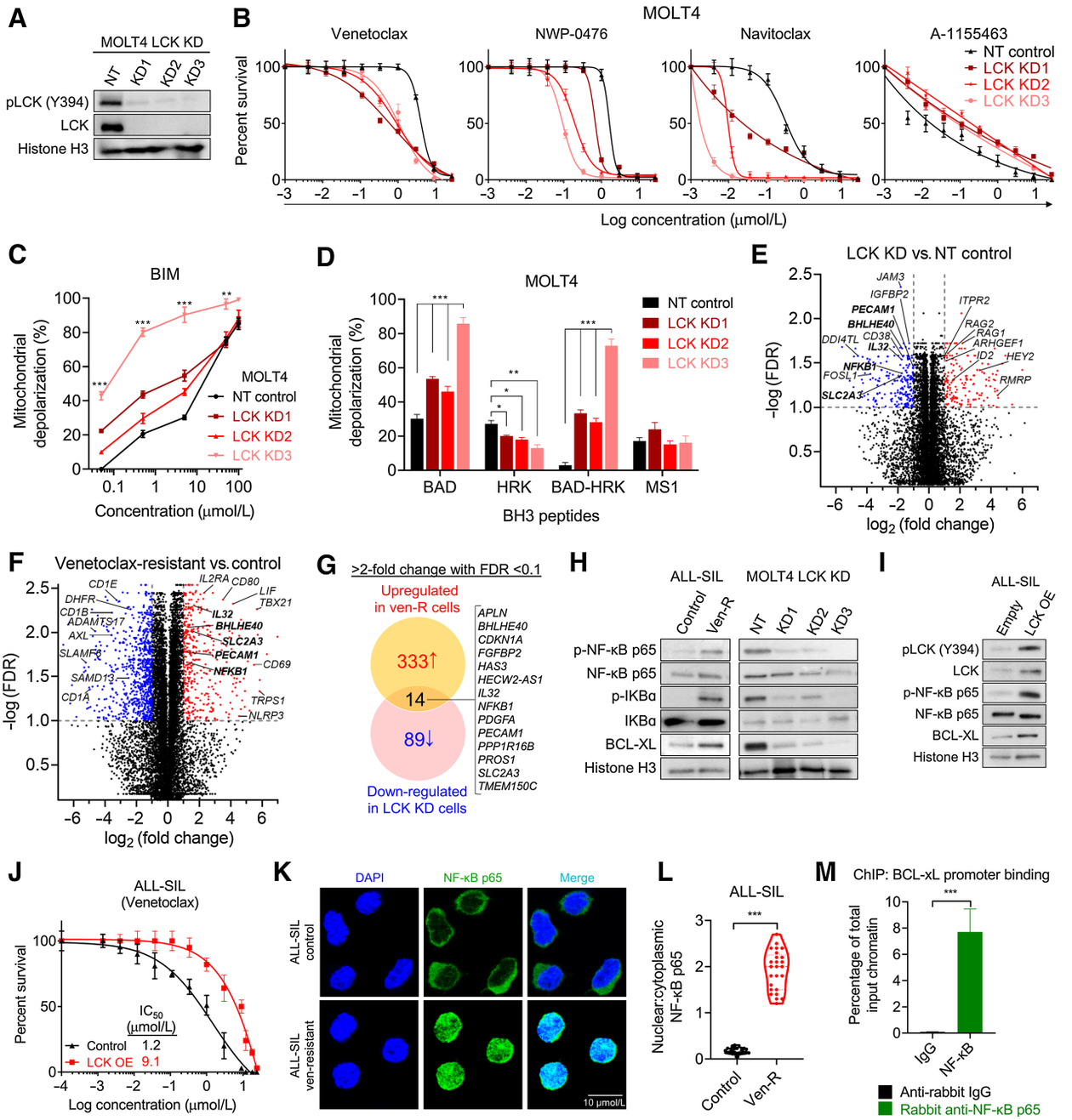

Figure 3.

LCK drives resistance to BCL-2 inhibition in T-ALL. **A,** Immunoblots showing LCK knockdown (KD) in MOLT4 T-ALL cell line. **B,** Curves showing viability of MOLT4 NT control and LCK KD cells treated with BH3 mimetics. **C,** BIM titration assay for MOLT4 NT control and LCK KD cells. **D,** BH3 profiling of MOLT4 NT control and LCK KD cells. **E,** Volcano plot showing differentially expressed genes between MOLT4 LCK KD versus NT control cells. **F,** Volcano plot showing differentially expressed genes between ALL-SIL ven-R versus control cells. **G,** Venn diagram showing genes that are upregulated in ven-R cells and downregulated in LCK KD cells. **H,** Immunoblots showing NF-κB pathway activity and BCL-xL expression levels in ven-R and LCK KD cells, compared with their respective controls. **I,** Immunoblots showing NF-κB pathway activity in ALL-SIL cells transduced with empty vector and LCK overexpression (OE) vector. **J,** Curves showing viability of ALL-SIL control and LCK OE cells treated with venetoclax. **K,** Immunofluorescence analysis of NF-κB staining in ALL-SIL control and ven-R cells. **L,** Violin plots showing nuclear:cytoplasmic ratio of NF-κB p65 staining. **M,** Bar graphs showing BCL-xL promoter binding of NF-κB p65 protein, assessed with ChIP of ALL-SIL ven-R cells (*, $P < 0.05$; **, $P < 0.01$; ***, $P < 0.001$).

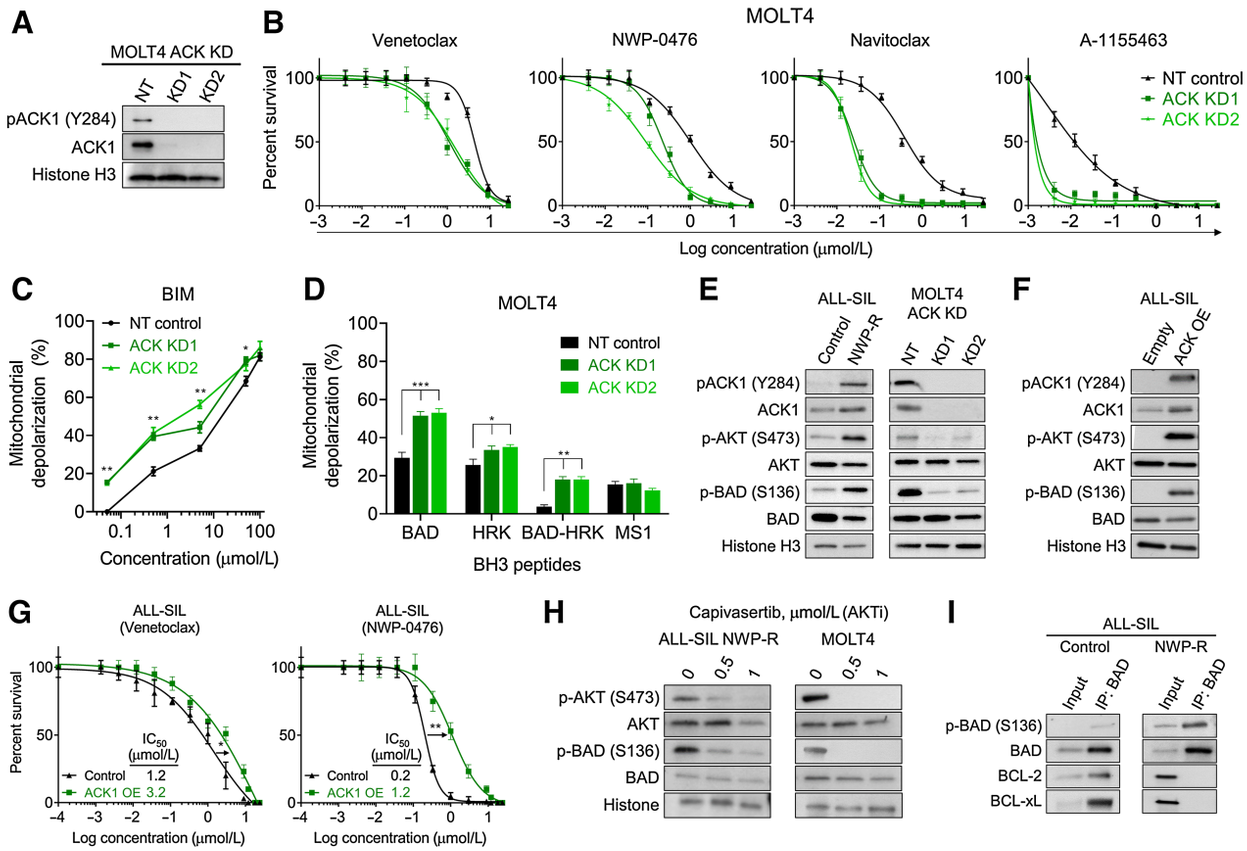

Figure 4.

ACK1 drives resistance to BCL-2 and BCL-xL inhibition in T-ALL. **A,** Immunoblots showing ACK1 knockdown (KD) in MOLT4 T-ALL cell line. **B,** Curves showing viability of MOLT4 NT control and ACK1 KD cells treated with BH3 mimetics. **C,** BIM titration assay for MOLT4 NT control and ACK1 KD cells. **D,** BH3 profiling of MOLT4 NT control and ACK1 KD cells. **E** and **F,** Immunoblots showing AKT pathway activity and BAD phosphorylation in NWP-R, ACK1 KD, and ACK1 overexpressing (OE) cells, compared with their respective controls. **G,** Curves showing viability of ALL-SIL empty vector control and ACK1 OE cells treated with BH3 mimetics. **H,** Immunoblots showing AKT pathway activity and BAD phosphorylation upon capivasertib treatment of ALL-SIL, NWP-R, and MOLT4 cells. **I,** Immunoblots showing BAD protein pulldown in ALL-SIL control and NWP-R cell lysates, probed with p-BAD, BAD, BCL-2, and BCL-xL (*, $P < 0.05$; **, $P < 0.01$; ***, $P < 0.001$).

S7F). Similarly, we observed synergy between venetoclax and ponatinib, and NWP-0476 and ponatinib in T-ALL primary cells (Supplementary Fig. S8A–S8C). Next, we investigated the combination of NWP-0476 plus dasatinib *in vivo* by engrafting NSG mice with luciferase-expressing T-ALL PDX cells, which were generated from the bone marrow sample of a relapsed T-ALL patient. At 1% engraftment, mice were treated in groups of 5 per arm: vehicle, NWP-0476 oral (50 mg/kg/day), dasatinib oral (30 mg/kg/day), and NWP-0476 plus dasatinib oral at same doses. Mice were treated for three weeks. Bioluminescence imaging revealed significantly reduced tumor burden in mice treated with the combination therapy when compared with the vehicle control or single-agent treatment groups (**Fig. 5C** and **D**). Mice treated with NWP-0476 plus dasatinib had decreased circulating T-ALL PDX cells and evidence of apoptosis in leukemic blasts (**Fig. 5E**). NWP-0476-treated mice had longer OS when compared with the vehicle control, and the combination treatment group had better OS than the mice in vehicle or single-agent therapy groups (**Fig. 5F**). Upon sacrifice, we harvested organs (liver, heart, kidneys, bowels) for toxicity assessment by two board-certified pathologists, who were blinded to the treatment groups of these mice (Supplementary Fig. S9A). Liver specimens from vehicle control mice contained high burden of leukemic infiltrates, and the combination therapy group had the lowest burden of disease. No significant hepatocyte toxicity was noted. We did not observe any significant cardiac, renal, or gastrointestinal toxicity. Taken together, we showed *in vitro* and *in vivo* synergy between BH3 mimetics and TKI therapy in aggressive T-ALL models, and the combination therapy was not associated with major organ toxicity in histopathologic examination.

Collectively, our findings demonstrate that LCK and ACK1 signaling pathways drive resistance to BCL-2 and BCL-xL inhibitors in T-ALL, and treatment with TKIs (dasatinib or ponatinib) can sensitize these tumors to BH3 mimetics (venetoclax or NWP-0476; **Fig. 6**).

Discussion

There is compelling biological and preclinical rationale, along with early-phase clinical data for targeting members of the BCL-2 family of proteins with BH3 mimetics in T-ALL (14, 24). However, there are limited data for the mechanisms of resistance that can be leveraged to improve the therapeutic efficacy of these agents. Given the paucity of treatment options for R/R T-ALL, new approaches and rationally designed combination strategies are urgently needed. In this study, we discovered the interplay between signaling and apoptotic pathways in T-ALL. Our data provide mechanistic insights into a signaling

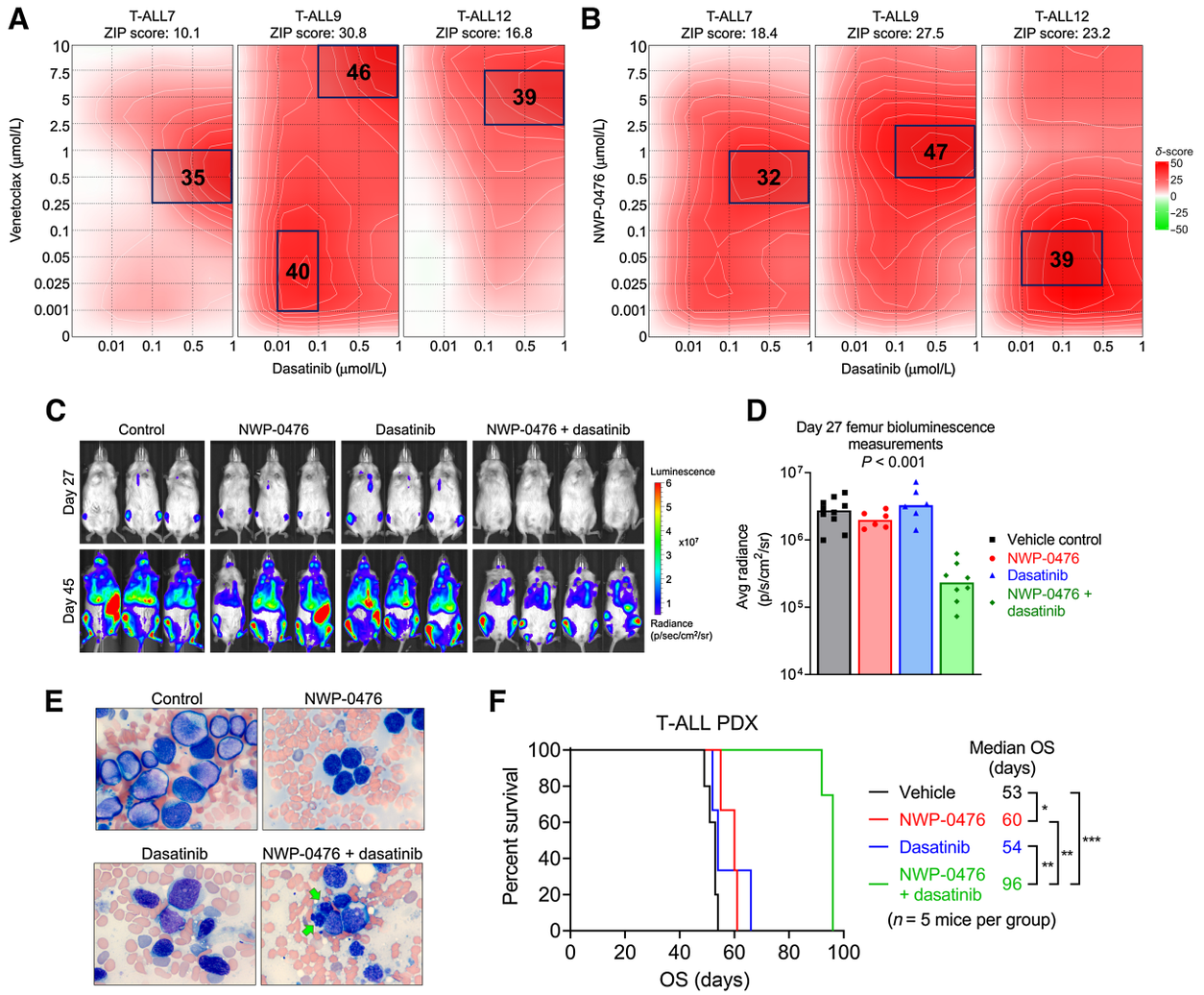

Figure 5.

Combination of BH3 mimetics and TKIs synergize in T-ALL. **A,** ZIP synergy plots of T-ALL primary cells treated with venetoclax and dasatinib. **B,** ZIP synergy plots of T-ALL primary cells treated with NWP-0476 and dasatinib. **C,** Bioluminescence imaging of NSG mice engrafted with luciferase-expressing T-ALL PDX cells. **D,** Bar graphs showing average bioluminescence measurements from femurs of mice on day 27. **E,** Blood smears of mice in different treatment groups, obtained on day 45. Arrows indicate blasts undergoing apoptosis. **F,** Kaplan–Meier OS curves of mice engrafted with T-ALL PDX cells and treated with vehicle control, oral NWP-0476, oral dasatinib, and oral NWP-0476 plus dasatinib combination (*, $P < 0.05$; **, $P < 0.01$; ***, $P < 0.001$).

network that regulates BCL-2 inhibitor resistance via NF-κB signaling and BCL-2/BCL-xL inhibitor resistance via ACK1–AKT signaling. Our functional studies demonstrate that silencing of LCK and ACK1 kinases change the BH3 profiles, and therefore BH3 mimetic sensitivities of T-ALL cells. In our preclinical studies, we observed that dasatinib (LCK and ACK1 inhibitor) sensitized an aggressive T-ALL PDX model to BCL-2/BCL-xL inhibition. Recent preclinical work also showed increased venetoclax resistance in T-ALL cells with high pre-TCR (LCK) signaling activity, suggesting a possible role for TKI therapy (25, 26). Our data provide sufficient preclinical evidence to investigate the NWP-0476 plus TKI (dasatinib or ponatinib) combination in a phase Ib/II feasibility study in R/R T-ALL, which is currently in development.

Venetoclax, a highly selective and orally bioavailable BCL-2 inhibitor, and navitoclax, an orally bioavailable BCL-2/BCL-xL inhibitor, induce apoptosis by releasing pro-apoptotic BAX and BAK proteins from these antiapoptotic proteins on mitochondrial surface (27–29). We recently helped to lead an early-phase clinical study demonstrating safety and efficacy of venetoclax and navitoclax when combined with low-dose chemotherapy in patients with R/R ALL (14). Despite the impressive CR rate of 53% in 19 R/R T-ALL patients treated on this study, most patients experienced rapid disease progression, suggesting emergence of BH3 mimetic resistance in this heavily pretreated patient population. The median OS was only 6.6 months and 1-year OS was 29%. In addition, delayed hematologic recovery was the primary safety finding, attributed to the on-target thrombocytopenia caused by navitoclax. NWP-0476 is a new orally bioavailable BCL-2/BCL-xL inhibitor with fine-tuned BCL-xL activity to minimize the platelet toxicity seen with other BCL-xL targeting agents. Our preclinical studies did not identify any major organ toxicity. A logical next step is to test the combination of NWP-0476 with TKIs targeting LCK and ACK1 signaling pathways.

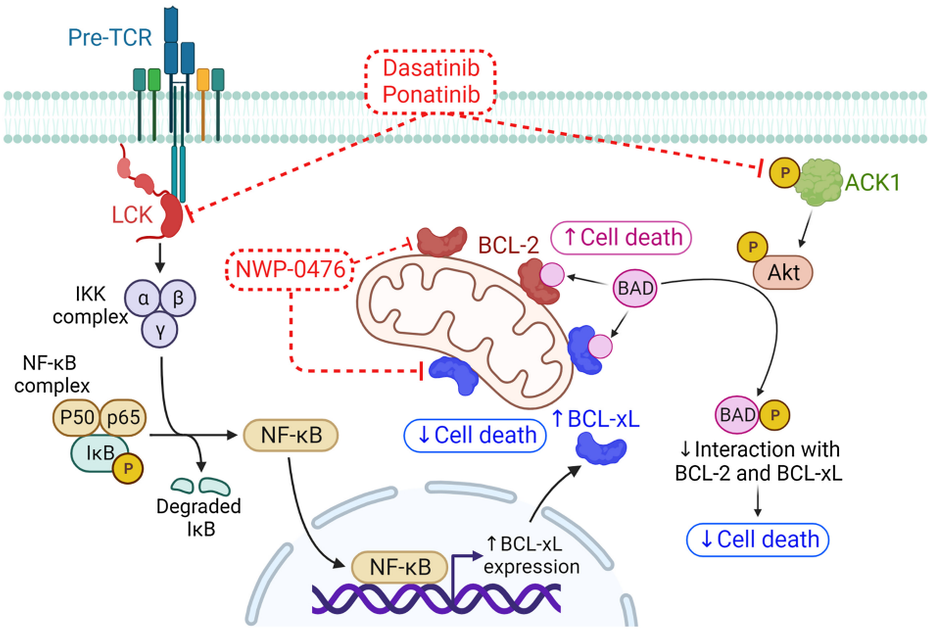

Figure 6.
LCK and ACK1 signaling pathways drive resistance to BH3 mimetics in T-ALL. (Created with BioRender.com.)

In conclusion, our findings establish LCK and ACK1 as critical BH3 mimetic resistance hubs that can be effectively targeted with dasatinib or ponatinib. Our results have immediate clinical applications and an early-phase clinical study investigating the combination of BH3 mimetics with TKI therapy is already underway (NCT05268003).

Authors' Disclosures

C. Saygin reports other support from Newave Pharmaceuticals during the conduct of the study. A. DuVall reports personal fees from CEConcepts outside the submitted work. A.A. Patel reports personal fees from AbbVie and Bristol Myers Squibb, as well as grants from Pfizer and Kronos Bio outside the submitted work. Y. Chen reports other support from Newave Pharmaceutical Inc. during the conduct of the study, as well as other support from Newave Pharmaceutical Inc. outside the submitted work. S.P. Anthony reports other support from Newave Pharmaceutical, Inc. outside the submitted work. Y. Chen reports other support from Newave Pharmaceutical Inc during the conduct of the study, as well as other support from Newave Pharmaceutical Inc. outside the submitted work. O. Odenike reports other support from Newave Pharmaceuticals during the conduct of the study; O. Odenike also reports grants from AstraZeneca, AbbVie, Astex, BMS, Incyte, Kartos, and Loxo, as well as personal fees from Servier, Kymera Therapeutics, Threadwell Therapeutics, Rigel, Blueprint Medicines, and Novartis outside the submitted work. D.T. Teachey reports grants from NIH during the conduct of the study; D.T. Teachey also reports other support from Sobi, as well as grants from NeoImmune Tech and BEAM Therapeutics outside the submitted work. J. LaBelle reports grants from AbbVie outside the submitted work. W. Stock reports personal fees and other support from Newave during the conduct of the study, as well as personal fees from Pfizer and Amgen outside the submitted work. No disclosures were reported by the other authors.

Authors' Contributions

C. Saygin: Conceptualization, data curation, formal analysis, writing–original draft, writing–review and editing. **G. Giordano:** Conceptualization, data curation. **K. Shimamoto:** Conceptualization, data curation. **B. Eisfelder:** Data curation, formal analysis, writing–review and editing. **A. Thomas-Toth:** Conceptualization, resources, data curation, writing–review and editing. **G. Venkataraman:** Conceptualization, resources, data curation, formal analysis, visualization. **V. Ananthanarayanan:** Conceptualization, data curation, visualization. **T.L. Vincent:** Conceptualization, resources, writing–review and editing. **A. DuVall:** Conceptualization, resources, writing–review and editing. **A.A. Patel:** Conceptualization, resources, writing–review and editing. **Y. Chen:** Resources. **F. Tan:** Resources. **S.P. Anthony:** Resources. **Y. Chen:** Resources. **Y. Shen:** Resources. **O. Odenike:** Conceptualization, project administration, writing–review and editing. **D.T. Teachey:** Conceptualization, resources, project administration, writing–review and editing. **B.L. Kee:** Conceptualization, project administration, writing–review and editing. **J. LaBelle:** Conceptualization, project administration, writing–review and editing. **W. Stock:** Conceptualization, resources, project administration, writing–review and editing.

Acknowledgments

C. Saygin was supported by the American Society of Hematology Research Training Award for Fellows, Conquer Cancer Foundation Young Investigator Award, Prevent Cancer Foundation Fellowship, Cancer Research Foundation Young Investigator Award, and the Leukemia Lymphoma Society Special Fellow Award. This work was also supported by the University of Chicago Comprehensive Cancer Center Pilot Project grant (to W. Stock) and an Investigator Initiated Clinical Trial grant (to C. Saygin, W. Stock). The authors thank Ms. Mary Beth Neilly for her assistance with Janet Rowley leukemia biorepository. BioRender was used to generate illustrations.

Note

Supplementary data for this article are available at Clinical Cancer Research Online (http://clincancerres.aacrjournals.org/).

Received February 10, 2023; revised May 8, 2023; accepted June 20, 2023; published first June 26, 2023.

References

1. Marks DI, Rowntree C. Management of adults with T-cell lymphoblastic leukemia. Blood 2017;129:1134–42.
2. Dunsmore KP, Winter SS, Devidas M, Wood BL, Esiashvili N, Chen Z, et al. Children's Oncology Group AALL0434: a phase III randomized clinical trial testing nelarabine in newly diagnosed T-cell acute lymphoblastic leukemia. J Clin Oncol 2020;38:3282–93.
3. Brown PA, Shah B, Advani A, Aoun P, Boyer MW, Burke PW, et al. Acute lymphoblastic leukemia, version 2.2021, NCCN Clinical Practice Guidelines in Oncology. J Natl Compr Canc Netw 2021;19:1079–109.
4. Roberts AW. Therapeutic development and current uses of BCL-2 inhibition. Hematology Am Soc Hematol Educ Program 2020;2020:1–9.

5. Letai AG. Diagnosing and exploiting cancer's addiction to blocks in apoptosis. Nat Rev Cancer 2008;8:121–32.
6. Kang MH, Reynolds CP. Bcl-2 inhibitors: targeting mitochondrial apoptotic pathways in cancer therapy. Clin Cancer Res 2009;15:1126–32.
7. DiNardo CD, Jonas BA, Pullarkat V, Thirman MJ, Garcia JS, Wei AH, et al. Azacitidine and venetoclax in previously untreated acute myeloid leukemia. N Engl J Med 2020;383:617–29.
8. Jain N, Keating M, Thompson P, Ferrajoli A, Burger J, Borthakur G, et al. Ibrutinib and venetoclax for first-line treatment of CLL. N Engl J Med 2019;380: 2095–103.
9. Le Gouill S, Morschhauser F, Chiron D, Bouabdallah K, Cartron G, Casasnovas O, et al. Ibrutinib, obinutuzumab, and venetoclax in relapsed and untreated patients with mantle cell lymphoma: a phase 1/2 trial. Blood 2021;137:877–87.
10. Kumar SK, Harrison SJ, Cavo M, de la Rubia J, Popat R, Gasparetto C, et al. Venetoclax or placebo in combination with bortezomib and dexamethasone in patients with relapsed or refractory multiple myeloma (BELLINI): a randomised, double-blind, multicentre, phase 3 trial. Lancet Oncol 2020;21:1630–42.
11. Balachander SB, Criscione SW, Byth KF, Cidado J, Adam A, Lewis P, et al. AZD4320, a dual inhibitor of Bcl-2 and Bcl-x(L), induces tumor regression in hematologic cancer models without dose-limiting thrombocytopenia. Clin Cancer Res 2020;26:6535–49.
12. Chonghaile TN, Roderick JE, Glenfield C, Ryan J, Sallan SE, Silverman LB, et al. Maturation stage of T-cell acute lymphoblastic leukemia determines BCL-2 versus BCL-XL dependence and sensitivity to ABT-199. Cancer Discov 2014;4: 1074–87.
13. Olesinski EA, Bhatia KS, Mahesh AN, Rosli S, Mohamed JS, Jen WY, et al. BH3 profiling identifies BCL-2 dependence in adult patients with early T-cell progenitor acute lymphoblastic leukemia. Blood Adv 2023;7:2917–23.
14. Pullarkat VA, Lacayo NJ, Jabbour E, Rubnitz JE, Bajel A, Laetsch TW, et al. Venetoclax and navitoclax in combination with chemotherapy in patients with relapsed or refractory acute lymphoblastic leukemia and lymphoblastic lymphoma. Cancer Discov 2021;11:1440–53.
15. Ravikrishnan J, Muhowski EM, Lai T-H, Misra S, Diaz Rohena D, Tan F, et al. Characterization of LP-118, a novel small molecule inhibitor of Bcl-2 and Bcl-Xl in chronic lymphocytic leukemia resistant to venetoclax. Blood 2021;138(Supplement 1):679.
16. Bride KL, Vincent TL, Im SY, Aplenc R, Barrett DM, Carroll WL, et al. Preclinical efficacy of daratumumab in T-cell acute lymphoblastic leukemia. Blood 2018; 131:995–9.
17. Eisfelder BJ, Saygin C, Wynne J, Colton MW, Fischietti M, Beauchamp EM, et al. OTS167 blocks FLT3 translation and synergizes with FLT3 inhibitors in FLT3 mutant acute myeloid leukemia. Blood Cancer J 2021;11:48.
18. Ludwig LM, Maxcy KL, LaBelle JL. Flow cytometry-based detection and analysis of BCL-2 family proteins and mitochondrial outer membrane permeabilization (MOMP). Methods Mol Biol 2019;1877:77–91.
19. Saygin C, Wiechert A, Rao VS, Alluri R, Connor E, Thiagarajan PS, et al. CD55 regulates self-renewal and cisplatin resistance in endometrioid tumors. J Exp Med 2017;214:2715–32.
20. Galaxy C. The Galaxy platform for accessible, reproducible and collaborative biomedical analyses: 2022 update. Nucleic Acids Res 2022;50:W345–51.
21. Mahajan K, Coppola D, Challa S, Fang B, Chen YA, Zhu W, et al. Ack1 mediated AKT/PKB tyrosine 176 phosphorylation regulates its activation. PLoS One 2010; 5:e9646.
22. Zhang T, Qu R, Chan S, Lai M, Tong L, Feng F, et al. Discovery of a novel third-generation EGFR inhibitor and identification of a potential combination strategy to overcome resistance. Mol Cancer 2020;19:90.
23. Datta SR, Dudek H, Tao X, Masters S, Fu H, Gotoh Y, et al. Akt phosphorylation of BAD couples survival signals to the cell-intrinsic death machinery. Cell 1997; 91:231–41.
24. Venugopal S, Kantarjian H, Short NJ, Thompson PA, Pemmaraju N, Jain N, et al. A phase II study of mini-hyper-CVD plus venetoclax in patients with philadelphia chromosome-negative acute lymphoblastic leukemia. Blood 2021;138: 1239.
25. Gocho Y, Liu J, Hu J, Yang W, Dharia NV, Zhang J, et al. Network-based systems pharmacology reveals heterogeneity in LCK and BCL2 signaling and therapeutic sensitivity of T-cell acute lymphoblastic leukemia. Nat Cancer 2021;2:284–99.
26. Laukkanen S, Veloso A, Yan C, Oksa L, Alpert EJ, Do D, et al. Therapeutic targeting of LCK tyrosine kinase and mTOR signaling in T-cell acute lymphoblastic leukemia. Blood 2022;140:1891–906.
27. Konopleva M, Letai A. BCL-2 inhibition in AML: an unexpected bonus? Blood 2018;132:1007–12.
28. Gibson CJ, Davids MS. BCL-2 antagonism to target the intrinsic mitochondrial pathway of apoptosis. Clin Cancer Res 2015;21:5021–9.
29. Brahmbhatt H, Oppermann S, Osterlund EJ, Leber B, Andrews DW. Molecular pathways: leveraging the BCL-2 interactome to kill cancer cells–mitochondrial outer membrane permeabilization and beyond. Clin Cancer Res 2015;21: 2671–6.